

# Computer-assisted analysis of *in-vitro* vasculogenesis and angiogenesis processes

Fabrizio Lamberti  
Politecnico di Torino  
Dip. di Automatica ed Informatica  
C.so Duca degli Abruzzi, 24  
I-10129, Torino, Italy  
lamberti@polito.it

Andrea Gamba  
Politecnico di Torino  
Dip. di Matematica  
C.so Duca degli Abruzzi, 24  
I-10129, Torino, Italy  
gamba@polito.it

Bartolomeo Montrucchio  
Politecnico di Torino  
Dip. di Automatica ed Informatica  
C.so Duca degli Abruzzi, 24  
I-10129, Torino, Italy  
montru@polito.it

## ABSTRACT

In recent years many experimental investigations have been carried out on vasculogenesis and angiogenesis, the mechanisms of blood vessels formation. Neovascularization is a hallmark of embryogenesis and many other physiological processes, such as wound healing or endometrium vascularization during the menstrual cycle. Angiogenesis also plays a key role in tumor growth, tumor metastasis and other pathological processes including many inflammatory diseases. Understanding biological phenomena regulating angiogenesis is therefore essential for clinical treatment of cancer and other angiogenesis-dependent diseases. This paper describes the development of a fully-automated computerized angiogenesis analysis system, which enables angiogenesis parameters to be quantified in an *in-vitro* model. The proposed methodology works on phase contrast microscopy snap photographs of cultured endothelial cell plates, and extracts a detailed graph-based representation of the blood vessels network thus supporting accurate angiogenesis parameters measurement.

## Keywords

Vasculogenesis, angiogenesis, analysis system, image segmentation, thinning, skeleton graph extraction.

## 1. INTRODUCTION

Neovascularization is defined as the sprouting of new blood vessels by expansion of the endothelium by proliferation, migration and remodeling [Car00a]. Neovascularization is fundamental to healing, reproduction as well as embryonic development. During development, new blood vessels originate by a process called *vasculogenesis* or are generated from pre-existing blood vessels by *angiogenesis*. Vasculogenesis and angiogenesis occur normally in the human body at specific times in development and growth. For example, a developing child in a mother's womb must create the vast network of arteries, veins, and capillaries that are found in the human body. Vasculogenesis creates the primary network of vascular endothelial cells that will

become major blood vessels. Later on, angiogenesis remodels this network into the small new blood vessels or capillaries that complete the child's circulatory system. Proliferation of new blood vessels also takes place in adults, although it is a relatively infrequent event. In women, angiogenesis is active a few days each month as new blood vessels form in the lining of the uterus during the menstrual cycle. Also, angiogenesis is necessary for the repair or regeneration of tissue during wound healing and plays a key role in tumor growth, tumor metastasis and other pathological processes [Car00b]. Understanding biological processes regulating vasculogenesis and angiogenesis is therefore essential for clinical treatment of cancer and other neovascularization-dependent diseases.

The ability to form networking capillary tubes is a cell autonomous property of endothelial cells (ECs). It is well known that culturing ECs on Matrigel, a preparation of basement membrane proteins, markedly accelerates their morphological differentiation in geometric tubular networks, which are almost identical to capillary vascular beds observed *in-vivo* [Kub88a]. In this way, the process of formation of a vascular network starting from randomly seeded cells can be accurately observed through videomicroscopy. Cells migrate over

Permission to make digital or hard copies of all or part of this work for personal or classroom use is granted without fee provided that copies are not made or distributed for profit or commercial advantage and that copies bear this notice and the full citation on the first page. To copy otherwise, or republish, to post on servers or to redistribute to lists, requires prior specific permission and/or a fee.

*Journal of WSCG, Vol.12, No.1-3, ISSN 1213-6972*  
WSCG'2004, February 2-6, 2003, Plzen, Czech Republic.  
Copyright UNION Agency Science Press

distances which are an order of magnitude larger than their radius and aggregate when they get in touch with one of their neighbors. In a time of the order of ten-twelve hours they form a continuous multicellular network. Several *in-vitro* vasculogenesis and angiogenesis models have been developed which have been proved to be effective in the study of neovascularization processes [Fol80a].

This paper describes the development of a fully-automated computerized angiogenesis analysis system, which enables the angiogenesis parameters to be quantified in an *in-vitro* model. Basically, the proposed methodology works on phase contrast microscopy snap photographs of cultured EC plates, and makes use of various image processing techniques in order to extract a detailed graph-based representation of the blood vessels network. Once such a formal representation is available, accurate angiogenesis factors measurement can be performed. The advantage of this system is that it easily and quickly provides reproducible results, making it suitable for supporting experimental studies on EC networks formation.

This paper is organized as follows: in Section 2 the overall organization of the proposed technique is presented. The following sections illustrate each image processing step in details. In particular, Section 3 presents a description of the segmentation step which allows to separate foreground information from background layer. Section 4 illustrates the thinning-based skeletonization process, which allows to extract essential structural information from the binary segmented image. Section 5 illustrates the procedure for graph-based representation extraction in details. Considerations on angiogenesis parameters measurement are reported in Section 6. Finally, in Section 7 results achieved using the proposed technique are presented and compared with experimental observations.

## 2. METHODOLOGY OVERVIEW

In *in-vitro* angiogenesis experimental observations, capillary patterns are mimicked by ECs cultured on basement membrane proteins. On this surface, single randomly dispersed cells (Figure 1a) organize to form a two dimensional network and later fold up creating a net of capillary-like chords (Figure 1b, c and d). The proposed computerized angiogenesis analysis system enables fully-automated processing of phase contrast microscopy snap photographs of such EC cultured plates thus providing an invaluable support to experimental studies on neovascularization. The overall methodology can be broken up into several consecutive steps which lead to the generation of a graph-based representation of the blood vessels network under investigation. Then,

essential angiogenesis parameters can be quickly and easily evaluated by referring to such formal representation.

The procedure is as follows. Human umbilical endothelial vein cells are cultured on Matrigel (ECM secreted by Engelbroth-Holm-Swarm sarcoma cells) a preparation of basement membrane proteins. Cells attach, migrate and assemble into irregular network of tubular structures radiating out from cell aggregates. Cells are observed with an inverted photomicroscope (model DM IRB HC; Leica Microsystems). Eight-bits 1024×1024 phase contrast snap photographs are taken with a cooled digital CCD Hamamatsu ORCA camera (Hamamatsu Photonic) several hours after seeding and digitally recorded. Microscopy photographs are segmented in order to obtain binary foreground images. Skeletonization is performed on segmented images so as to extract a thinned image conveying essential structural information in a relatively small number of pixels. A formal graph-based description of the cell network is then extracted from such a graphical representation by using an adaptation of breadth-first search. Data collected during graph-based representation generation are then used to compute capillary chords length in order to validate the accuracy of the proposed automated technique.

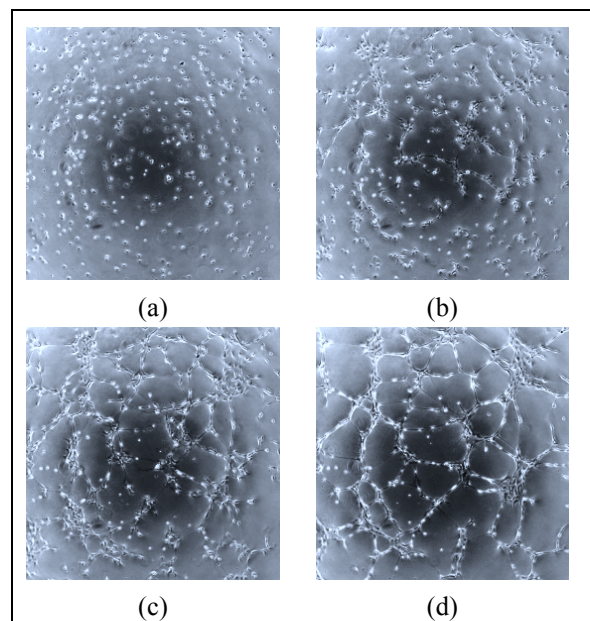


**Figure 1. Capillary-like network formation by human umbilical ECs: a) 0 hours. b) 1.5 hours. c) 3 hours. d) 6 hours after seeding.**

## 3. IMAGE SEGMENTATION

Segmentation is defined as the process of partitioning an image into several constituent components, distinguishing features of interest from background

[Pal93a]. Segmentation allows to reduce image complexity for further analysis and therefore plays a key role in any automated image processing system.

To handle the complexity of the particular images under consideration, an ad-hoc segmentation technique has been developed by keeping into particular account biological characteristics derived from experimental observations carried out on angiogenesis phenomena. Several steps can be identified. First a thresholding technique is applied in order to extract all those pixels for which the probability of belonging to the foreground is sufficiently high. For this, two thresholds  $t_l$  and  $t_h$  have been experimentally defined in order to separate very bright and very dark structures. Pixels whose gray value is below  $t_l$  or above  $t_h$  are painted black (foreground) in the output image containing segmentation result. Since medial axis of blood vessels generated by self-assembly of endothelial cells appears darker than vessel contours and vessel contours are somewhat smoothed, a higher  $t_l$  and a lower  $t_h$  have been used to process those pixel for which the number of immediate neighbors (8-neighborhood) already belonging to the segmented image is greater or equal to two. In this way, connectivity is preserved and smoother boundaries are obtained. Selected thresholds proved to be effective for segmenting all test images. However, in the future we expect to evaluate the effect of more sophisticated adaptive thresholding techniques.

Then, a gradient-based technique has been applied to process those pixel for which classification is more delicate. It should be observed that vessels are generally characterized by regular linear orientations. Moreover, there exists vessels which are characterized by soft gray variations with respect to the background. Keeping in mind these considerations, a specific multi-oriented gradient-based technique enabling accurate discrimination between foreground and background pixels has been designed. In the following, the algorithm for vertical-like direction is presented. The extension to the horizontal-like case is straightforward.

For each pixel in the input image, nine gradients are computed for each pixel in a  $3 \times 3$  kernel centered in the considered pixel. Gradient  $g(i,j)$  is defined as  $g(i,j) = \text{abs}(c(i,j) - c(i-1,j))$  where  $c(i,j)$  is the gray value of the pixel in position  $(i,j)$ . A threshold  $g_t$  has been defined. The computed gradient matrix is compared with the gradient masks in Figure 2 (dark gray boxes mean  $g(i,j) > g_t$ ). When template is matched, central pixel is added to the foreground set and painted black in the output image. Figure 3 shows pixel configurations producing gradient matrices matching vertical-like oriented gradient templates.

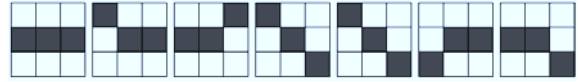


**Figure 2. Gradient masks for vertical-like oriented gradient-based segmentation step (gray box means  $g(i,j) > g_t$ ). Oriented gradient matrix obtained for current pixel is compared with each gradient mask. When template is matched, current pixel is added to the foreground.**

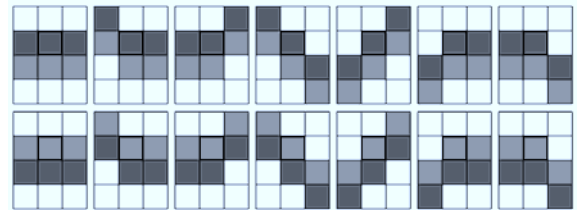


**Figure 3. Pixel configurations producing gradient matrices matching vertical-like oriented gradient templates (central pixel of  $3 \times 3$  kernel is highlighted).**

A predefined set of postprocessing steps including opening, closing and smoothing operations is finally applied on the output image in order to close up breaks in features, opening spaces between just touching figures and making vessel contours softer.

Segmentation of microscopy photograph in Figure 4 is illustrated in Figure 5.

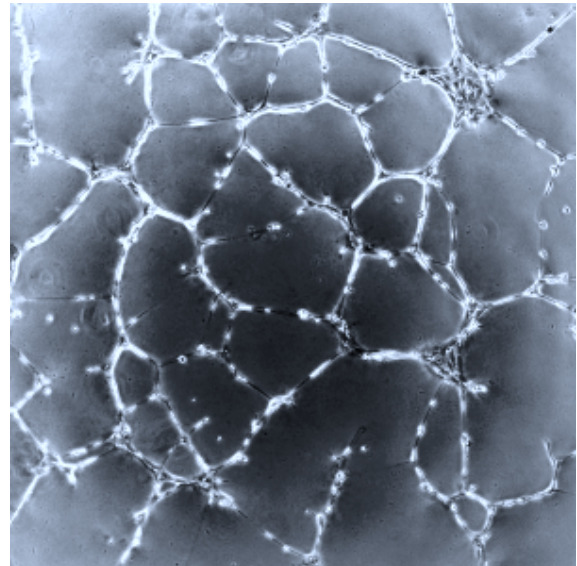


**Figure 4. Endothelial cells network. ECs were plated ( $125 \text{ cells/mm}^2$ ) on Matrigel and phase contrast snap photograph of a  $4 \text{ mm}^2$  wide portion of surface was taken 12 hours after seeding.**

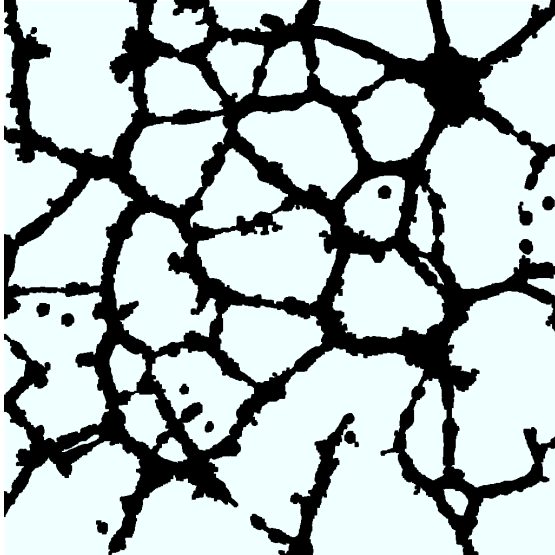


**Figure 5. Binary image obtained with the proposed segmentation procedure ( $t_l=30$ ,  $t_h=220$  and  $g_l=5$ ). White is background.**

#### 4. SKELETONIZATION

A *skeleton* is presumed to represent the shape of an object in a relatively small number of pixels, all of which are in some sense structural and therefore necessary. Skeletonization, therefore, is defined as the act of identifying those pixels belonging to an object that are essential for communicating the object's shape: these are skeletal pixels, and form a set, the skeleton. The skeletonization step has been deployed using a thinning-based approach. The majority of thinning algorithms are based on a repeated stripping away of layers of pixels until no more layers can be removed. There is a set of rules defining which pixels may be removed, and frequently some sort of template-matching scheme is used to implement these rules. In this work, we selected well-established Zhang-Suen implementation [Zha84a] which is capable of producing a sufficiently accurate skeleton. The algorithm is broken up into two subiterations. In one iteration a pixel  $I(i,j)$  is marked for deletion if the following four conditions are all true:

1. its connectivity number is one;
2. it has at least two black neighbors and not more than six;
3. at least one of  $I(i,j+1)$ ,  $I(i-1,j)$  and  $I(i,j-1)$  are background (white);
4. at least one of  $I(i-1,j)$ ,  $I(i+1,j)$  and  $I(i,j-1)$  are background.

The connectivity number is a measure of how many objects a particular pixel might connect. One such measure is  $C_n = \sum_{k \in S} N_k - (N_k \cdot N_{k+1} \cdot N_{k+2})$  where  $N_k$  is the color value of one of the eight neighbors of the

pixel involved and  $S=\{1,3,5,7\}$ .  $N_l$  is the color value of the pixel to the right of the central pixel, and they are numbered in counterclockwise order around the center. The value of  $N_k$  is one if the pixel is white (background) and zero if black (object). The center pixel is  $N_o$ , and  $N_k = N_{k-8}$  if  $k > 8$ .

At the end of this subiteration the marked pixels are deleted. The next subiteration is the same except for steps 3 and 4. Pixel is marked for deletion if

1. its connectivity number is one;
2. it has at least two black neighbors and not more than six;
3. at least one of  $I(i-1,j)$ ,  $I(i,j+1)$  and  $I(i+1,j)$  are background (white);
4. at least one of  $I(i,j+1)$ ,  $I(i+1,j)$  and  $I(i,j-1)$  are background.

and again, any marked pixels are deleted. If at the end of either subiteration there are no pixels to be deleted, then the skeleton is complete, and the algorithm stops.

There are some problems with thinning algorithms that show up as artifacts in the skeleton. The first of these is called *necking*, in which a narrow point at the intersection of two lines is stretched into a small line segment. Also, *tails* can be created where not exist because of excess thinning where two lines meet at an acute angle. Finally, *hairs* or *line fuzzes* (the creation of extra line segments joining a real skeleton segment) frequently appear.

We adopted a preprocessing stage proposed by Stentiford [Ste83a] which allows to minimize these thinning artifacts. Since line fuzz is frequently caused by small irregularities in the object outline, a smoothing step is applied before thinning to remove them. Basically, a pass is made over all pixels, deleting those having two or fewer black neighbors and having a connectivity number less than two. For dealing with necking, *acute angle emphasis* procedure is applied, in which all pixels near the joint between two lines are set to white if they plug up a acute angle.

Finally, since sometimes, when thinning is complete, there are still pixels that could be deleted (principal among these are pixels that form a staircase) we use Holt's staircase removal [Hol87a] which allows half of the pixels in a staircase to be removed without affecting the shape of connectedness of the overall object by applying a template-matching technique.

Figure 6 shows the skeleton image resulting from the application of our hybrid implementation based on the merging of those three methods in the following order: Stentiford's preprocessing scheme feeding images into Zhang-Suen's basic algorithm, with Holt's staircase removal as a post-processor.

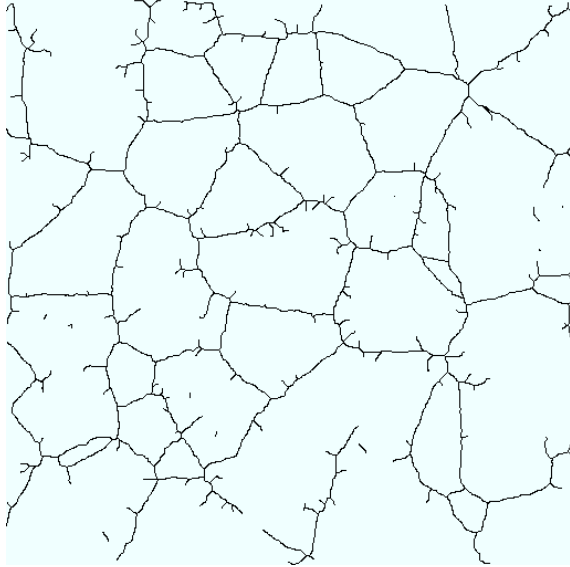


**Figure 6. Skeleton obtained by applying the proposed hybrid thinning procedure to segmented image in Figure 5.**

## 5. GRAPH EXTRACTION

We developed an image-based technique enabling the extraction of a detailed graph-based representation of the blood vessels network from a skeleton image. The availability of such a representation constitutes the basis for accurate angiogenesis parameters measurement.

An adaptation of the breadth-first search (BFS) algorithm was used. Given a graph  $G=(V,E)$  where  $V$  is the vertex set and  $E$  the edge set, original BFS systematically explores the edges of  $G$  to discover every vertex that is reachable from  $s$  (where  $s$  is a distinguished source vertex) producing a breadth-first tree with root  $s$  that contains all such reachable vertices. The BFS procedure normally assumes the existence of an input graph  $G$  represented by means of an adjacency list. Moreover, it relies on the selection of source vertex  $v$ . Here, only a graphical representation of the graph (the skeleton image) is available and the creation of a sophisticated adjacency list maintaining information regarding vertex reachability as well as edges related information is the actual goal of the automated algorithm. Furthermore, the concept of vertex in such a graphical graph representation has to be defined in a suitable manner. Finally, at least one source vertex has to be identified in the graphical graph representation. It has to be remarked that a single skeleton image can originate more than one breadth-search tree and, as a consequence, the selection of more than one source vertex may be required. In the following, template based rules for vertex recognition and the BFS-like technique for graph extraction are presented.

### Vertex recognition

We defined the following rules to establish whether a pixel belonging to the skeleton should be considered a vertex of the graph or not. First, the number  $n$  of skeleton pixels in a  $3 \times 3$  grid centered in the considered vertex is computed. The discrimination criterion is as follows:

- $n < 2$ :  $p$  is a vertex;
- $n=2$ :  $p$  is a vertex iff neighboring pixels are adjacent;
- $n=3$ :  $p$  is a vertex iff there not exist a pair of adjacent neighboring pixels;
- $n=4$ :  $p$  is a vertex iff there not exist more than one pair of adjacent neighboring pixels;
- $n > 4$ :  $p$  is a vertex;

This criterion is illustrated in Figure 7. Possible configurations for  $n = \{0,1,2,3,4\}$  are shown in details. The extension to  $n = \{5,6,7,8\}$  is straightforward.

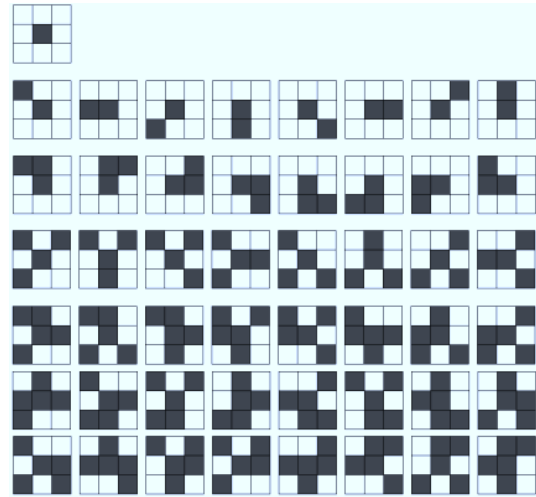


**Figure 7. Illustration of the template based technique for vertex recognition.  $3 \times 3$  grids for  $n = \{0,1,2,3,4\}$  neighbors satisfying conditions for being a vertex.**

### Breadth-first search

First, an initial source vertex  $s$  has to be identified. The input image is visited beginning from the top-left corner. As soon as a pixel belonging to the skeleton is reached, the algorithm applies the available rules in order to establish if the current pixel should be considered a vertex. If not, that means that an edge of the graph has been reached. The algorithm moves along that edge until a vertex is reached. When the first vertex is discovered, modified BFS implementation can be used since a source vertex is available. Like the basic BFS, the proposed implementation relies on a first-in, first-out queue  $Q$  to maintain vertices that have still to be processed. Furthermore, the proposed

implementation keeps track of progress by coloring each visited vertex and edge using a specific color representing its state. In the initialization step, vertex  $s$  is added to the empty queue  $Q$  as well as to the adjacency list. Then, a loop is executed which iterates as long as there remain vertices to be processed in  $Q$ . The vertex at the head of  $Q$  is considered and its neighboring pixels (8-neighborhood) belonging to the skeleton are painted gray. As long as there exists neighboring gray pixels, one of this pixels is considered. This pixel represents the initial point of an edge leaving the current vertex. An edge is therefore added to current vertex. The algorithm follows the edge until a node is reached, adding pixels to the edge. If the vertex has not yet been discovered, the vertex is added to the queue and to the adjacency list as well. The execution continues with the remaining neighboring gray pixels of the current vertex. Once the edges originating from each gray neighboring pixel has been considered, current vertex is removed from  $Q$  and the following vertex in the queue is considered. Visited edges and vertices are canceled in the input image as soon as they have been discovered. When all the vertices in  $Q$  have been considered, a partial adjacency list representing a breadth-first tree is available. This procedure is repeated as long as source vertices can be found in the input image. At the end, an adjacency list containing all the vertices together with pixels belonging to the edges leaving each vertex for the whole image is generated. Note that this step allows only to identify all those edges leaving from a particular vertex. Since our aim is the creation of an undirected graph, a post-processing step is performed in order to complete the adjacency list. That is, for each node, for each leaving edge an entering edge is created by inverting the pixels constituting the leaving edge. Modified implementation of the BFS procedure is illustrated in Figure 8. A graphical representation of the formal graph description obtained using modified BFS is shown in Figure 9.

### Pruning

Most of the artifacts produced by basic thinning algorithms are removed by introducing preprocessing and postprocessing steps in the skeletonization procedure. Nevertheless, several line fuzzes which do not actually represent any structural feature in the segmented objects are still present in the skeleton (Figure 10.a, 10.b). A pruning operation is therefore performed in order to remove these artifacts (Figure 10.c). This procedure is repeated until no branches longer than 20 pixels remain in the image. Removed edges and vertices are marked as dead in the adjacency list. As a consequence of the pruning operation, several vertices with two leaving live edges remain in the graph, which do not satisfy the

rules for being a vertex anymore. These vertices and edges are removed from the adjacency list and new undirected edges are created as the collection of constituting canceled edges (Figure 10.d and 12).

```

while  $s \leftarrow FindSource()$ 
   $Enqueue(Adj,s)$ 
   $Enqueue(Q,s)$ 
  while  $Q \neq \emptyset$ 
     $v \leftarrow head[Q]$ 
    for each  $n \in neighbors[v]$ 
       $u \leftarrow AddEdge(v)$ 
       $p \leftarrow n$ 
       $AddPoint(u,p)$ 
      while  $IsVertex(p) \neq true$ 
         $p \leftarrow MoveToNeighbor(p)$ 
         $AddPoint(u,p)$ 
      if  $p \notin Adj$  then
         $Enqueue(Q,p)$ 
     $Dequeue(Q)$ 

```

Figure 8. Procedure for graph extraction.

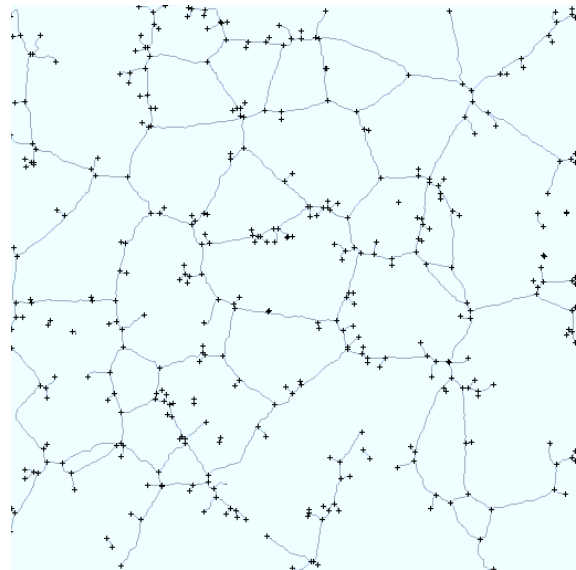
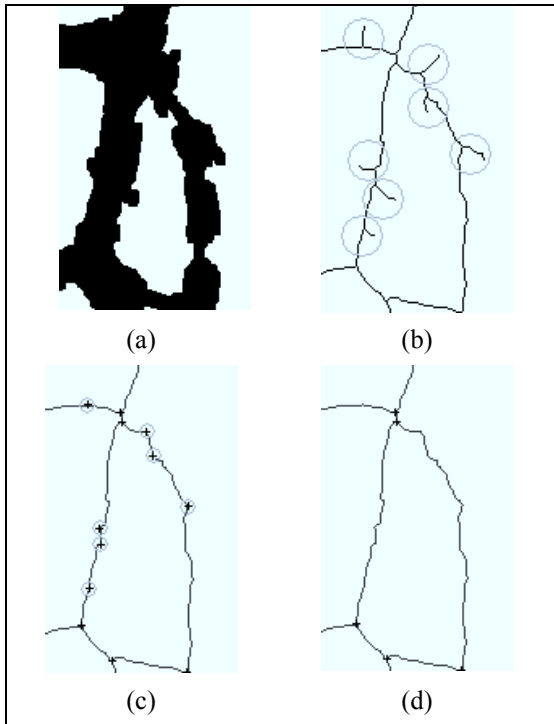


Figure 9. Representation of formal graph.

## 6. MEASUREMENTS

The ordered list of skeleton pixels constituting each edge of the undirected graph is collected in the process of extracting the graph. This information has been used to perform edge length measurements. Several length measurement techniques have been evaluated. We first defined  $\ell_1$  as the sum of the pixels constituting the edge. The main drawback of this measure is that it underestimates the actual length of the edge. This is mainly due to the fact that this technique does not take into account the relative position of consecutive pixels. Therefore we

investigated the effectiveness of more accurate measurement techniques based on length estimators derived from a characterization of the discrete curve representing the edge. For this, we selected the most used length estimator which has been presented in [Dor87]. According to this approach, we defined  $\ell_2(n_e, n_o) = 0,948n_e + 1,343n_o$  where  $n_e$  is the number of vertical and horizontal chain elements and  $n_o$  is the number of diagonal chain elements of the edge. We experienced that the major disadvantage of this technique is that it is too sensitive to small fluctuations around the median axis of the skeletonized edge. This translates into an overestimation of the actual length of the edge.



**Figure 10. Details of the pruning procedure. a) Binary segmented image. b) Skeleton (circles indicate line fuzz artifacts originated by the thinning algorithm). c) Graph-based representation reconstructed from the adjacency list after pruning step (circles indicate vertex which have to be removed from adjacency list together with leaving edges). d) Graph-based representation after removal of irregular vertices and edges (canceled edges are replaced by new edges being the aggregation of constituting edges).**

For this reason, we proposed an alternative technique which is capable of compensating the discrete nature of edge shapes. We defined  $\ell_3(\delta)$  as the sum of the Euclidean lengths of  $\delta$ -pixels segments constituting the edge. Finally,  $\ell_4(\delta)$  has been defined as the

average of  $\ell_3(\delta)$  lengths measured on the same edge by varying the starting pixel of the second segment between 1 and  $\delta-1$ . The third technique is more accurate with respect to the previous ones. Nevertheless, results achievable by means of this method can be improved using the fourth technique, which makes the dependence on the actual shape of the edge being considered negligible.

For each edge in the graph, length measures using the fourth technique have been computed and stored in the adjacency list. An example of application of the aforementioned techniques on the sample edge in Figure 11.a together with achieved measurement results are shown in Figures 11.b, c, d. In the future, we expect to evaluate the accuracy of additional measurement techniques.

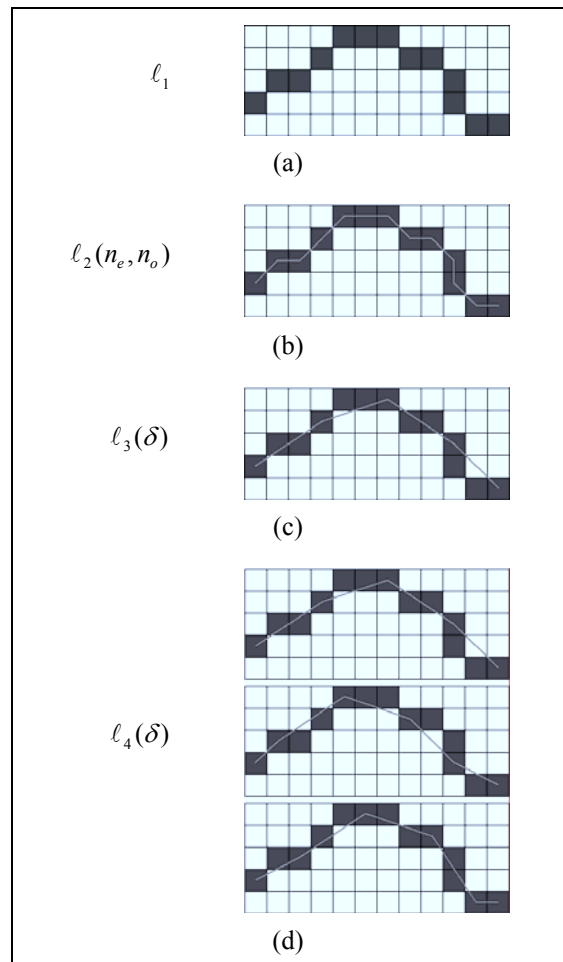


**Figure 11. Example of computation of edge lengths using  $\delta=4$ . a)  $\ell_1=13$ . b)  $\ell_2(n_e, n_o)=13,75$ . c)  $\ell_3(\delta)=13,21$ . d)  $\ell_4(\delta)=13,49$ .**

## 7. RESULTS AND DISCUSSION

As shown in Section 6, in order to evaluate the accuracy of the proposed computer assisted analysis technique, collected data has been processed to

obtain a measure of vessels length, an essential angiogenesis parameter which consistence can be easily verified by means of a comparison with results achieved in other experimental observations.

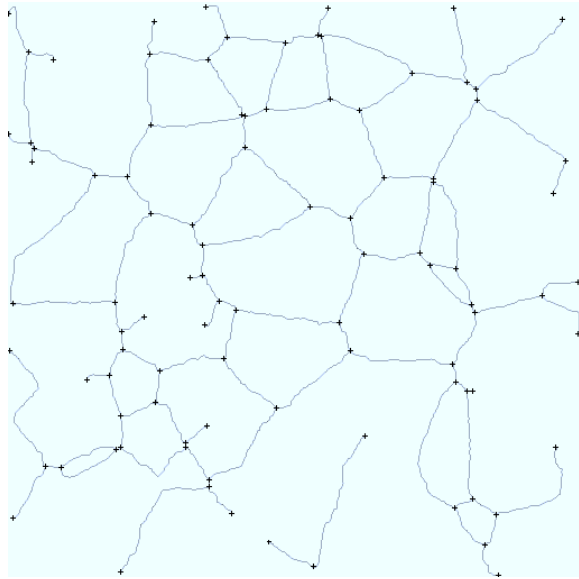


**Figure 12. Formal graph after pruning step.**

For this purpose, human endothelial cells from umbilical cord veins were prepared, characterized and cultured as described in [Gam03a]. Twenty-four-well culture plates (2 cm<sup>2</sup> growth area/well; Becton Dickinson) were coated with 0.3 ml of Matrigel (8.8 mg/ml; Becton Dickinson), which was then allowed to solidify at 37° C. Endothelial cells were then released from culture plates using trypsin/EDTA, pelleted, counted, resuspended in medium at the appropriate cell dilution, and added to Matrigel-coated wells. Cells were incubated at 37° C in a 5% CO<sub>2</sub> humidified atmosphere for 12-14 hours. During time-lapse videomicroscopy constant temperature (37° C) and CO<sub>2</sub> (5%) were maintained throughout the experiment by means of a heatable stage and a climate chamber. Phase contrast snap photographs of ten different plates were taken twelve hours after seeding and digitally recorded. The segmentation procedure presented in Section 3 has been applied to each recorded snap photograph and binary foreground images have been obtained. Skeletons have been computed for each segmented image using the thinning algorithm described in Section 4. Cells network graph based description has been obtained for each skeleton as illustrated in Section 5. Finally, length measurements have been performed on collected data how described in Section 6. In accordance with experimental observations in [Gam03a], it has been verified that the mean chord length measured by applying the aforementioned techniques on graph edges is  $\bar{\ell} \approx 200\mu\text{m}$  (and it is

independent on the initial cell density  $\bar{n}$  for  $\bar{n}$  between 100 to 200 cells/mm<sup>2</sup>).

Other characteristic angiogenesis parameters can be easily observed and quantified in a reproducible fashion by processing blood vessels network geometric information recorded in the formal graph-based description extracted by means of the proposed methodology. The developed technique proved to be an effective instrument for supporting experimental studies on neovascularization processes.

## 8. ACKNOWLEDGMENTS

We thank G. Serini and the Institute for Cancer Research and Treatment (IRCC, Candiolo, Torino) for kindly providing us with their experimental data.

## 9. REFERENCES

- [Car00a] Carmeliet, P. Mechanisms of angiogenesis and arteriogenesis. *Nature medicine* 6, Nature Publishing Group, pp. 389-395, 2000.
- [Car00b] Carmeliet P. and Rakesh, K.J. Angiogenesis in cancer and other diseases. *Nature* 407. NPS, pp. 249-257, 2000.
- [Dor87] Dorst, L. and Smeulders, A.W. Length estimators for digitized contours. *CVGIP* 40, pp. 311-333, 1987.
- [Fol80a] Folkman, J., Haudenschild, C. Angiogenesis in vitro. *Nature* 288, Nature Publishing Group, pp. 551-556, 1980.
- [Gam03a] Gamba, A., Ambrosi, D., Coniglio, A. De Candia, A., Di Talia, S., Giraud, E., Serini, G., Preziosi, L., Bussolino, F. Percolation, morphogenesis, and burgers dynamics in blood vessels formation. *Phys. Rev. Lett.* 90, 2003.
- [Hol87a] Holt, C.M., Stewart, A., Clint, M. and Perrott, R.H., An improved parallel thinning algorithm. *Com. of ACM* 30, No. 2, pp. 156-160, 1987.
- [Kub88a] Kubota, Y., Kleinman, H.K., Martin, G.R., Lawley, T.J. Role of laminin and basement membrane in the morphological differentiation of human endothelial cells into capillary-like structures. *Journal of Cell Biology* 107, Rockefeller Univ. Press, pp.1589-1598, 1988.
- [Pal93a] Pal, N.R. and Pal, S.K. A review of image segmentation techniques. *Pattern Recognition* 26, pp. 1277-1294, 1993.
- [Ste83a] Stentiford, F.W.M. and Mortimer, R.G. Some new heuristics for thinning binary handprinted characters for OCR. *IEEE Trans. on Systems, Man, and Cyb.* 13, No.1, pp. 81-84, 1983.
- [Zha84a] Zhang, S. and Fu, K.S. A thinning algorithm for discrete binary images. in *Int. Conf. in Comp. and App. conf. proc.*, Beijing, China. pp. 879-886, 1984.